




Design and analysis of planar four-port UWB-MIMO antenna with band-rejection capability

Harleen Kaur¹, Hari Shankar Singh^{1,2}  and Rahul Upadhyay¹

¹Department of Electronics and Communication Engineering, Thapar Institute of Engineering and Technology, Patiala, India and ²TIET-VT Center of Excellence for Emerging Materials, TIET, Patiala, India

Research Paper

Cite this article: Kaur H, Singh HS, Upadhyay R (2024) Design and analysis of planar four-port UWB-MIMO antenna with band-rejection capability. *International Journal of Microwave and Wireless Technologies* **16**(1), 127–139. <https://doi.org/10.1017/S175907872300065X>

Received: 10 August 2022
Revised: 25 April 2023
Accepted: 1 May 2023

Keywords:

band-notch; channel capacity loss; diversity gain; envelop correlation coefficients; impedance bandwidth; mean effective gain; multiple-input multiple-output; mutual coupling; ultra-wideband

Corresponding author: Hari Shankar Singh;
Email: harishankar1990@gmail.com

Abstract

This manuscript presents a 50Ω microstrip-fed quad-element high isolated ultra-wideband (UWB) multiple-input multiple-output (MIMO) antenna with band-notched characteristics. The overall area of the proposed structure is $0.33\lambda_0 \times 0.33\lambda_0 \text{ mm}^2$ (where λ_0 depicts the free space wavelength corresponding to the lower cutoff frequency, i.e. 2.54 GHz), etched on an FR-4 substrate of thickness 0.8 mm. The top layer has four semicircular disc-shaped radiating elements that are identical and orthogonal to obtain better inter-element isolation and compactness. A reverse two-shaped slot is etched onto the radiating patches to attain a band-rejection capability. Moreover, a decoupling structure is also placed at the top layer to suppress the unwanted surface waves. The bottom layer consists of a ground plane, which is further modified with quasi-self complementary and meandered line slots. A rectangular slot is also etched below the feed line to better match the impedance near the lower cutoff frequencies. The simulated reflection coefficients (S_{11}) of the proposed antenna are less than -10 dB over 2.54 to 10.74 GHz frequencies except at 3.37 to 4.15 GHz (WiMAX/C band), and the simulated inter-port isolation (S_{21}) is greater than -15 dB over the entire UWB range of frequencies (3.1 to 10.6 GHz). Also, the measured S-parameter results well agreed with the simulated ones. Furthermore, the simulation study of the 20-element UWB-MIMO antenna is also investigated using the proposed quad-element structure.

Introduction

Ever since an unlicensed band for ultra-wideband (UWB) communication (3.1–10.6 GHz) is allocated by the Federal Communications Commission, numerous UWB-based systems have been rapidly developing [1]. Much literature is available on the design challenges and implementation of UWB antennas. The technology covers a vast range of applications in different domains, including medical devices, mobile communications, and nowadays, Internet of Things-based gadgets [2–4]. However, multipath fading has always been considered as a significant problem in UWB systems [5], due to which UWB multiple-input multiple-output (MIMO) technology came into the picture and has attracted many researchers in academia and industry. It offers intriguing features like fading mitigation, data rate enhancement, and channel capacity without additional power consumption. However, when the mutual coupling rate of nearby exciting elements increases, the antenna's performance parameters badly deteriorate. Hence, one of the major challenges of MIMO antenna systems is to increase inter-element isolation [6]. In fact, to further vary the isolation level between radiating elements, utilization of already reported methods such as placement of decoupling and matching networks [7], neutralization lines [8], electromagnetic bandgap (EBG) structures [9], defected ground structures (DGS) [10], and parasitic elements [11] can be done. Recently, meta-material-inspired and fractal antennas are also investigated for UWB-MIMO applications [12, 13]. However, they often complicate the design geometry. One of the most efficient ways to attain high inter-element isolation is by positioning all the elements orthogonally.

In [14], the authors presented a high isolated dual-element triangular-shaped MIMO antenna with two step cut at its lower edge for UWB wireless communication applications. In addition, two F-shaped stubs were introduced in the ground plane to enhance isolation between radiators. The authors also discussed some important diversity parameters such as envelope correlation coefficients ($ECC < 0.04$) and diversity gain ($DG > 7.4 \text{ dB}$). Likewise, in [15], the authors analyzed a compact dual-element half-cutting UWB-MIMO antennas with fence-shaped decoupling structure in the ground. This fence structure comprised 16 slits, worked as a band-stop filter to attain high isolation between radiating elements. However, the antenna size in both articles is relatively large compared to the proposed design. Meanwhile, few

Table 1. Comparison of the proposed antenna with other antennas

References	Size (mm ³)	Overall volume	Ports	Operating frequency (GHz)	Transmission coefficients (dB)	Efficiency in most of the band (%)	Band-notched
[14]	50 × 30 × 1.6	2400	2	2.5 to 14.5	≤-20	90	-
[15]	50 × 35 × 1.0	1750	2	3 to 11	≤-25	-	-
[16]	42 × 25 × 1.6	4830	4	3.1 to 12	≤-22	80	-
[17]	31 × 31 × 1.6	1537	4	2 to 10.6	≤-15	70	-
[18] ^a	31.5 × 34 × 0.8	856	4	3.1 to 10.8	≤-25	80	Dual
[19]	40 × 23 × 1.5	1380	2	2.5 to 10.4	≤-25	-	Single
[20]	23 × 40 × 1.6	1472	2	2 to 11	≤-17	80	Triple
[21] ^b	26 × 15 × 1.6	624	2	3.1 to 35	≤-24	85	Dual
Proposed work	39 × 39 × 0.8	1216	4	2.54 to 10.74 GHz	≤-15	75	Dual

^a In practice, the ground plane in the case of the MIMO antenna should always be connected.

^b Size of the reported antenna is small; impedance bandwidth is quite large but consists of two ports.

researchers have started working with four-port antennas to attain better diversity performance. In [16], a high isolated compact four-port antenna without any decoupling network is discussed. Four different 50 Ω microstrip lines (MTLs) and four grounded stepped slot radiating elements are utilized in this design. High level of inter-element isolation is attained because of slot antenna's inherent directional radiative nature and asymmetrical positioning. Further, in [17], authors also analyzed a compact high isolated four-port UWB-MIMO antenna for wireless applications. A quasi-ellipse quad-element UWB-MIMO antenna with a protuberant ground is presented. The designed antenna has ECC < 0.005 and DG > 9.97. Despite mutual coupling, another major concern in the UWB-MIMO antenna is the interference caused by existing wireless standard bands (Wi-Fi, WiMAX, C, WLAN, and X-band). In view of these issues, researchers have been investigating the performance characteristics of UWB-MIMO antenna with band-reject capabilities [18–21]. In [18], a quad-element dual band-notch UWB-MIMO antenna with two different configuration is reported. In design-I, four orthogonally arranged F-shaped radiators are utilized. Band-notch at 7.3 GHz is attained with a pair of mushroom-type EBG structures, while folded U-shaped slot is responsible for creating notch at 8.2 GHz; while in design-II, a quad-element cuboidal MIMO antenna is studied. Furthermore, in [19], a reconfigurable MIMO antenna with band-reject properties for WLAN band is analyzed. The design has two complementary stepped rectangular-shaped monopoles, each combined with the quadrant-shape structure. A rectangular DGS at the ground controls the impedance matching over the frequencies of interest. High isolation is realized with a slotted circular-type ring grounded element. The reconfigurable band-reject properties were attained only with the switches in the main radiator that activate or deactivate the slots. Then in [20], a compact triple-band-notch (WiMAX, WLAN, and X-band) dual-port UWB-MIMO antenna using single cell two-via compact EBG is designed. An inverted L-type ground stub suppresses the surface wave coupling. Also in [21], a dual-element UWB-MIMO antenna with dual band-reject characteristics is examined. The antenna rejects WLAN band (5.09–5.8 GHz) and the IEEE INSAT/Super-Extended C band (6.3–7.27 GHz) with upper and lower L-shaped slits, respectively. Also, an inverted L-shaped decoupling structure in the ground enhances the inter-port isolation. The detailed

comparison (in terms of size, impedance bandwidth, isolation technique, and diversity parameters) between some already published UWB-MIMO manuscripts and the proposed antenna is highlighted in Table 1.

This article contains a compact quad-element MIMO antenna for UWB wireless applications. The design includes four semicircular-shaped radiating patches fed by four different modified microstrip feed lines. All are placed in orthogonal arrangement so that each radiator is at 90° about the other. Along with the radiators, a decoupling structure is also placed at the top layer to achieve better results, while on the other side of the substrate, a quasi-self complementary (QSC) technique is used in the ground plane along with the meandered line slits. Furthermore, a rectangular slot is etched to improve the impedance bandwidth of the proposed antenna. Finally, a reverse two-shaped slot is etched into each radiating element, creating a band-notched at the WiMAX (3.3 to 3.7 GHz) and downlink C band (3.7 to 4.2 GHz). It is observed that the proposed diversity antenna offers good impedance matching performance, as well as high isolation over the operating band of frequencies. The manuscript has been further categorized into five sections: configuration of the designed antenna, results and analysis that includes radiation and diversity performance, the investigation of the three-dimensional UWB-MIMO antenna, and the conclusion.

Antenna configuration and evolution

Single-port UWB antennas

Figure 1(a) shows the top and bottom layers of the proposed single-port antenna without slot, whereas Fig. 1(b) depicts the top and bottom layers of the design with slot. The top radiating patches comprise a semicircular disc, which is excited using a stepped 50 Ω MTL and integrated on the FR-4 substrate (having $\epsilon_r = 4.4$, $\tan\delta = 0.02$). To attain better impedance matching characteristics over the UWB range of frequencies, the ground plane of the proposed antenna has been modified with a QSC slot and two different rectangular slots. The optimized design parameters are $L = 23$ mm, $W = 14.5$ mm, $l_1 = 8.5$ mm, $l_2 = 7$ mm, $w = 1.5$ mm, $g = 1$ mm, $h = 5.75$ mm, $a = 7$ mm, $b = 3.1$ mm, $c = 9.45$ mm, $d = 4$ mm, $e = 8.25$ mm, and $r = 6.5$ mm. Figure 1(c) illustrates the zoomed view of the single radiating element of the proposed

antenna. A reverse two-shaped slot has been introduced in the radiating elements to notch the interfering C band. The optimized design parameters of the slots are $n = 0.25$ mm, $m = 3.3$ mm, $p = 8.5$ mm, $j = 3.75$ mm, and $k = 1.75$ mm. Figure 1(d) show the S-parameters in dB of the proposed antenna with and without slot. The results reveal that the reflection coefficients (S_{11}) of the proposed antenna have values less than -10 dB over frequencies 3.63 to 11.04 GHz without slot. However, the proposed structure with slot reveals S_{11} values of less than -10 dB over frequencies varying from 3.59 to 10.83 GHz except at 3.74 to 4.21 GHz (notching a C band from UWB). Further, Fig. 1(e) shows the realized gain and total efficiency of the proposed antenna with and without slot. It is observed that both gain and efficiency of the proposed antenna remain unvaried from 1.36 to 3.91 dB and 76 to 92% over the operating frequencies, respectively, but this highly degrades in the C-notched band with the introduction of slot.

UWB-MIMO antenna without band-notch characteristics

Further, in Fig. 2(a), MIMO configuration is introduced where four metallic semicircular disc-shaped radiating elements fed with four different modified 50Ω MTLs and a decoupling structure is utilized, while Fig. 2(b) depicts the bottom side of the substrate in which QSC slots along with the meandered lines slots are etched in the ground plane to attain the desired results. In addition, another rectangular slot has also been introduced in the ground to achieve good impedance matching over the operating frequency band. The dimensions of the radiating element are approximately chosen as $\lambda/4$ (~ 24 mm) at 3.1 GHz (lower cut off frequency), and the structure is resonating at 3.1 GHz corresponding to electrical length. The overall volume of the proposed UWB-MIMO antenna is $39 \times 39 \times 0.8$ mm³. The antenna elements are excited by four stepped MTLs and are positioned orthogonal toward each other to attain better inter-element isolation and compactness in the structure. The working impedance bandwidth of the proposed antenna varies from 2.62 to 10.73 GHz. Satisfactory inter-element isolation of more than -13 dB and -15 dB is observed over the UWB band between adjacent elements (e.g. port-1 and port-2) and diagonal elements (e.g. port-1 and port-3), respectively. Figure 2(c) illustrates the simulated S-parameters of the proposed quad-element UWB-MIMO antenna. Further, the parametric analysis of the proposed antenna has been carried out to validate the result of S-parameters. The following are the optimized design parameters: $L_x = 39$ mm, $L_y = 39$ mm, $a = 6.5$ mm, $c_1 = 1.55$ mm, $c_2 = 9.45$ mm, $c_3 = 15.65$ mm, $c_4 = 2.65$ mm, $c_5 = 5.65$ mm, $l_1 = 7$ mm, $l_2 = 0.5$ mm, $w = 1.5$ mm, $g = 1$ mm, $r = 6.5$ mm, $g_1 = 8.25$ mm, $g_2 = 13.5$ mm, $g_3 = 9.5$ mm, $g_4 = 7.37$ mm, $g_5 = 0.25$ mm, $g_6 = 2.1$ mm, and $g_7 = 3.1$ mm.

UWB-MIMO antenna with band-notch characteristics

This section discusses how the proposed antenna attains a band-reject capability. Figure 3(a) and (b) shows the top and bottom layout of the proposed UWB-MIMO resonator with band-notched capability, respectively. The basic idea is that the etched slot acts as a quarter-wavelength ($\lambda_g/4$) resonator whose dimensions can be mathematically obtained from the following equations [22]:

$$L_n = m + p = 11.8, \tag{1}$$

$$L_n \cong \frac{\lambda_g}{4} = \frac{c}{4f_n \sqrt{\epsilon_{reff}}} = 11.794mm \tag{2}$$

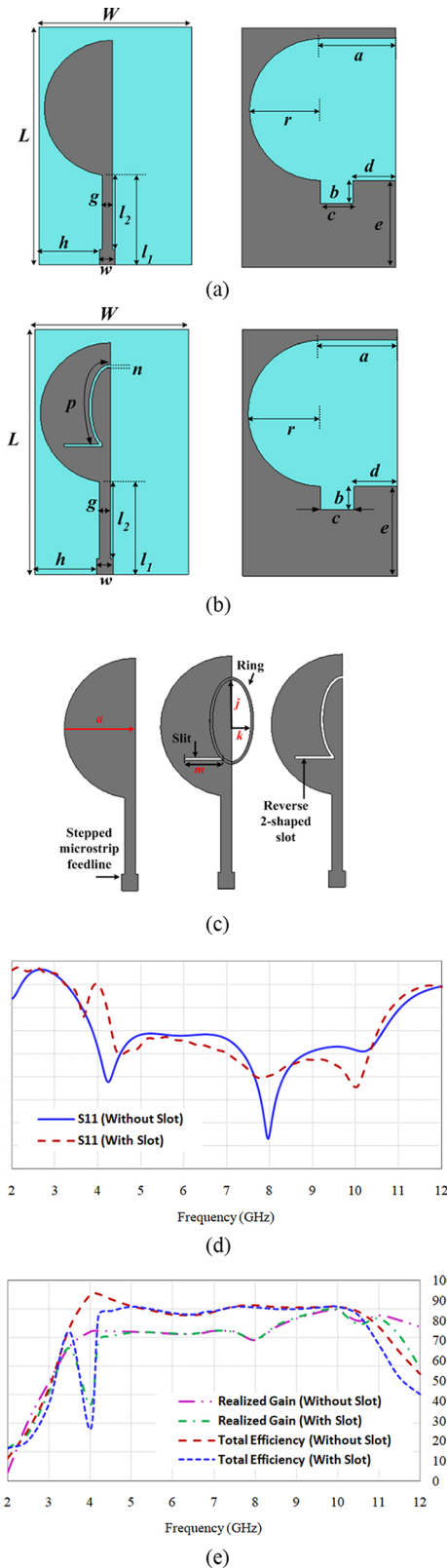


Figure 1. (a) Top and bottom layout of the proposed single-element UWB antenna without slot. (b) Top and bottom layout of the proposed single-element UWB antenna with slot. (c) Zoomed view of the single radiating element of the proposed antenna. (d) Simulated reflection coefficients of the proposed single-element UWB antenna with and without slot. (e) Simulated realized gain and total efficiency of the proposed single-element UWB antenna with and without slot.

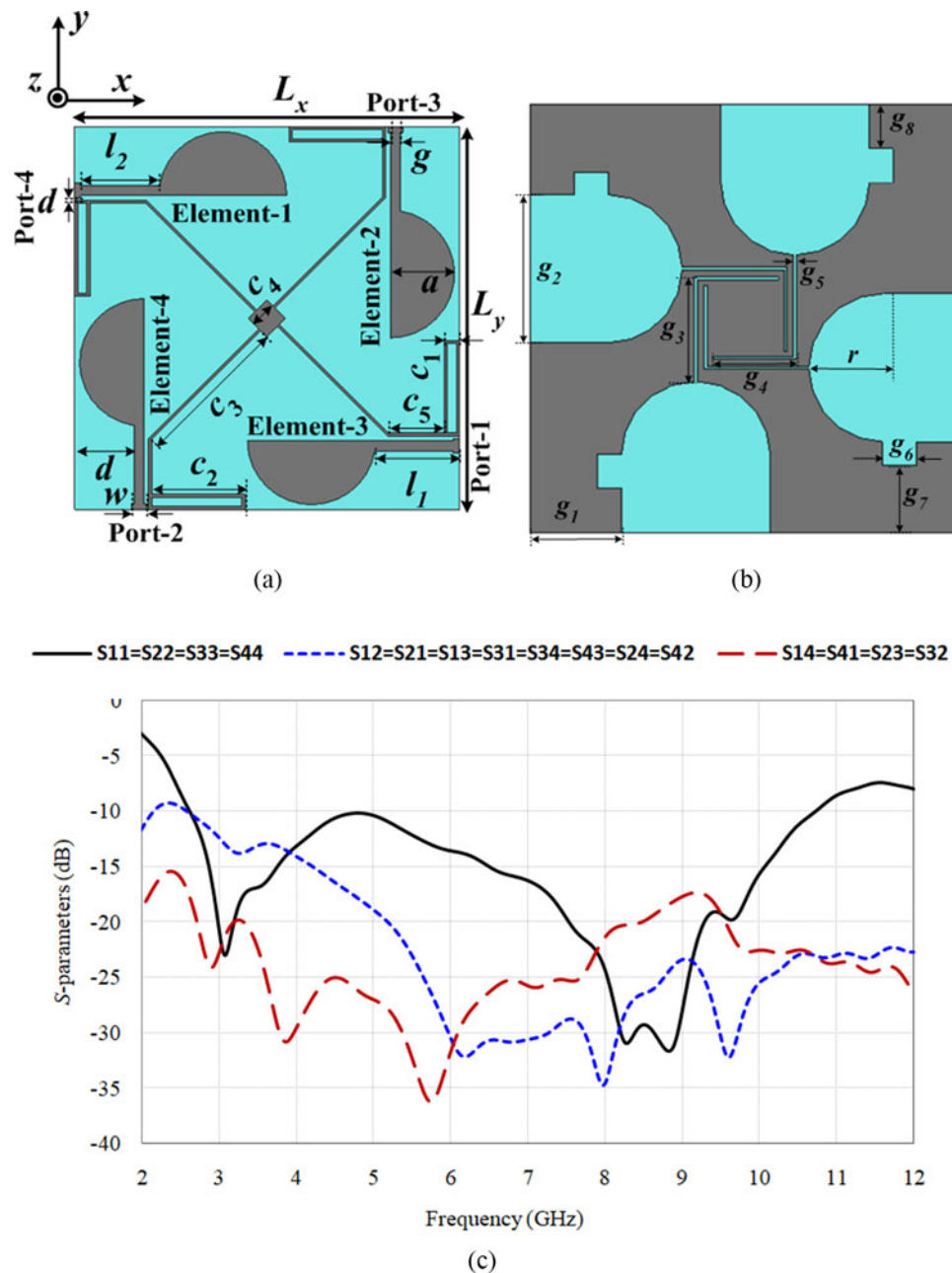


Figure 2. (a) Top layout of the proposed UWB-MIMO antenna. (b) Bottom layout of the proposed UWB-MIMO antenna. (c) Simulated S-parameters of the proposed antenna.

where “ c ” and $\epsilon_{\text{reff}} = ((\epsilon_r + 1)/2)$ denote the speed of light in meters per second and the effective dielectric constant, respectively. “ L_n ” is the optimized length of the reverse two-shaped slot and “ f_n ” is the simulated stop-band resonating frequency of the proposed antenna. The optimized value of length “ L_n ” is chosen as 11.8 mm, whose corresponding notched frequency obtained using Eq. (1) provides stop-band resonance at 3.87 GHz, and full-wave simulation exhibits the stop-band characteristics at 3.86 GHz. It can be noted that the simulated and computed values of quarter-wave size reverse two-shaped slit are responsible for suppressing the interfering WiMAX/C band (3.37 to 4.15 GHz).

Further, Fig. 3(c) depicts the simulated S-parameters of the proposed antenna. Its reflection coefficients are less than -10 dB

over 2.54–10.74 GHz except at a notched band (3.86 GHz) with excellent inter-element isolation (between diagonal and adjacent antenna elements) of more than -15 dB over the entire UWB operating band ranging from 3.1 to 10.6 GHz. To better illustrate the effect of a reverse two-shaped slot on radiation, the surface current distribution plots of the proposed antenna are analyzed. Figure 4(a) and (b) shows the surface current plots of the proposed antenna with and without a reverse two-shaped slot, respectively. While measuring the radiation patterns of any MIMO antenna, only one of the elements is made to radiate at a time while others are matched and terminated at 50Ω load. Both adjacent and diagonal elements develop these induced currents. It is interestingly noted from Fig. 4(a) that the proposed antenna without a reverse two-shaped slot has non-zero net radiation at a frequency

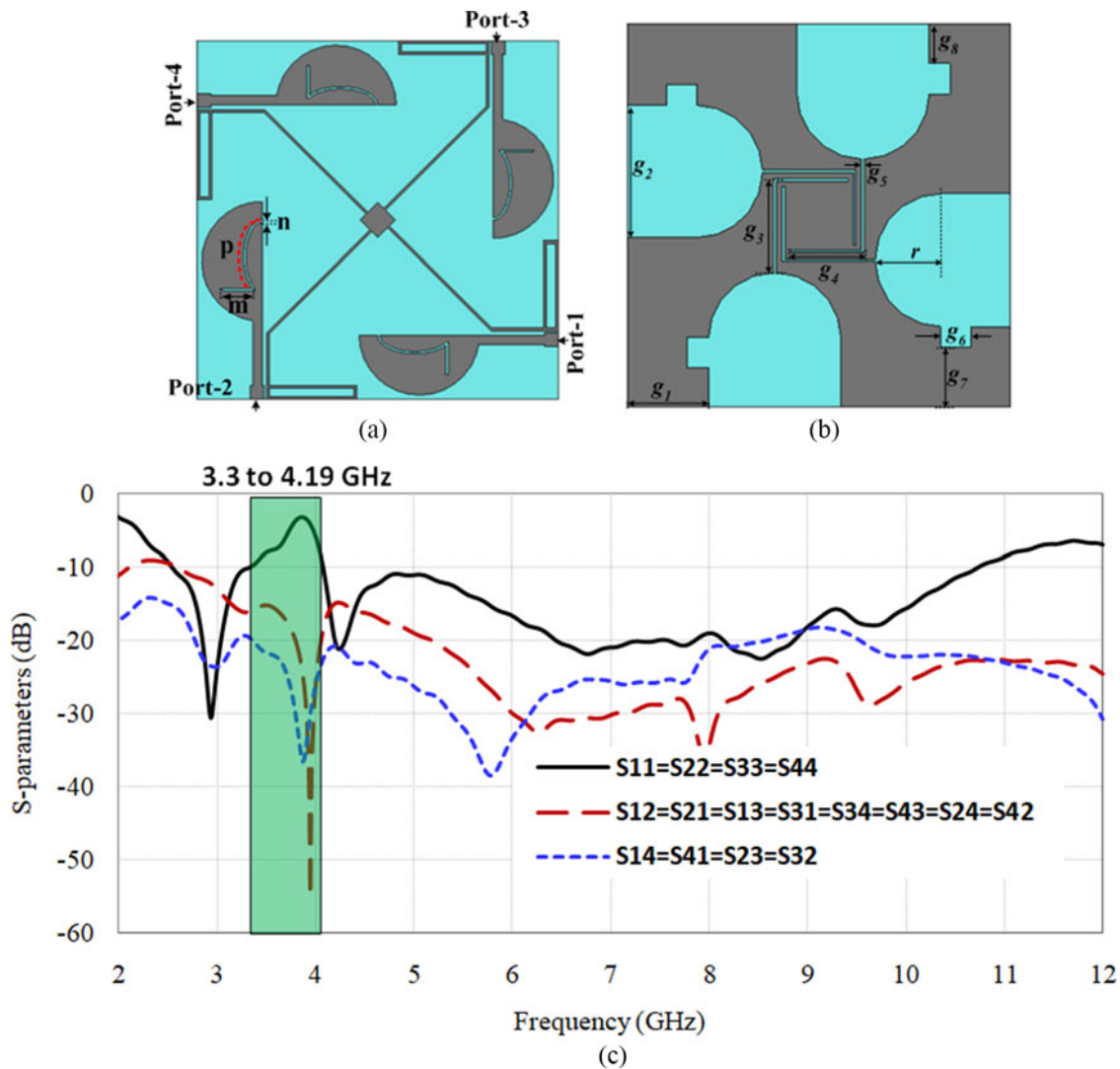


Figure 3. (a) Top layer of the proposed antenna with band-notched characteristics. (b) Bottom layer of the proposed antenna with band-notched characteristics. (c) Simulated S-parameters of the proposed antenna with band-notched characteristics.

of 3.86 GHz. However, in the case of the reverse two-shaped slot as shown in Fig. 4(b), most of the generated current at notched frequency 3.86 GHz is concentrated around the slot etched on the radiator. Hence, the net resultant current traveling in opposite directions nullifies each other, thereby suppressing the current path due to the $\lambda/4$ slot, creating a notch at the WiMAX/C band.

Design analysis of the proposed antenna

In this section, the importance of the stepped feed line, meandered line slot, and rectangular slot in the proposed design is well explained. Figure 5(a) depicts the S-parameters of the proposed band-notched UWB-MIMO antenna with and without stepped feeding line. Figure 5(b) highlights the S-parameters of the proposed band-notched UWB-MIMO antenna with and without rectangular slot etched in the ground. Figure 5(c) illustrates the S-parameters of the proposed band-notched UWB-MIMO antenna with and without meandered line grounded slot. Clearly when the stepped feed line is introduced, the cutoff frequencies do not show any significant variation. However, some impedance mismatch

exists around 10 GHz. Further, without rectangular slot etched in the ground creates poor impedance matching around 5 to 9 GHz. Furthermore, the meandered line slits are embedded in the ground to obtain the desired UWB band. Without them, the lower resonating frequencies get shifted. In addition, these degrade the reflection coefficients. It is also noted that the effect of introducing stepped MTL, rectangular slot, and meandered line slot on transmission coefficients remain almost insignificant.

Results and discussions

Reflection coefficient and radiation characteristics

To better justify the rationality of the proposed antenna, fabrication of the prototype and testing has been done. Figure 6(a) and (b) depicts the fabricated prototype (front and back side) and snapshot of the S_{11} and S_{21} , respectively. For testing, a vector network analyzer of series Keysight E5063A (100 kHz–18 GHz) is connected to the antenna under test where only one port is excited while the other ports are terminated with a matched load of 50Ω . The observed S-parameters of the proposed antenna with

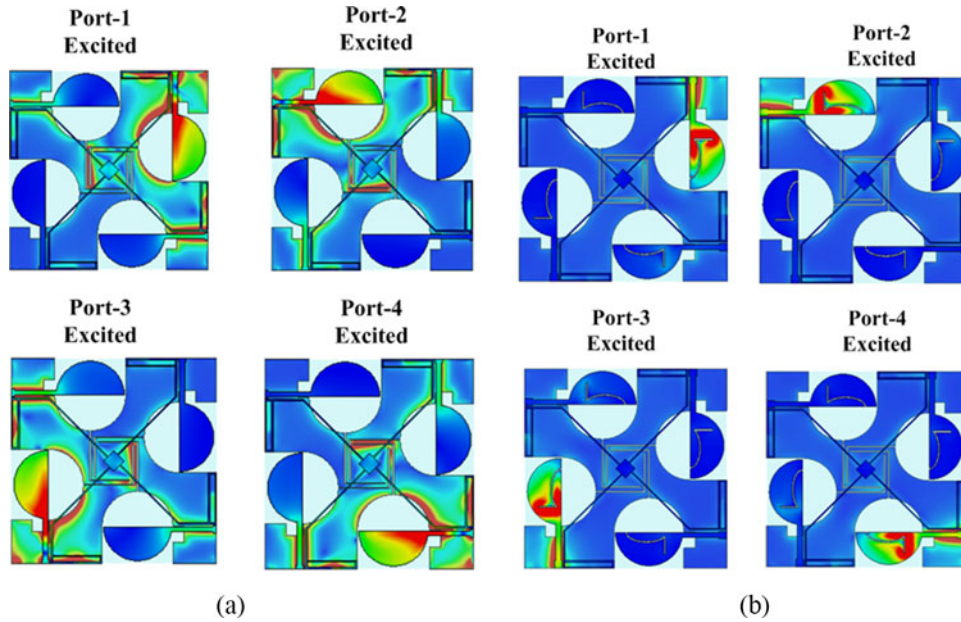


Figure 4. (a) Surface current distribution of the proposed antenna without reverse two-shaped slot at frequency 3.86 GHz. (b) Surface current distribution of the proposed antenna with reverse two-shaped slot at frequency 3.86 GHz.

band-notched characteristics are satisfactory with the simulated *S*-parameters results. The measured and simulated reflection coefficients (in dB) are compared in Fig. 6(c). It is noted that the measured S_{11} , S_{22} , S_{33} , and S_{44} of port-1, port-2, port-3, and Port-4 are slightly different due to testing inaccuracies or nonuniform fabrication of elements. Further, Fig. 6(d) depicts the measured and simulated transmission coefficients (in dB). The plot shows that the isolation between the adjacent (S_{12} , S_{13} , S_{21} , S_{24} , S_{31} , S_{34} , S_{42} , and S_{43}) and diagonal elements (S_{14} , S_{23} , S_{41} , and S_{32}) well agrees with each other due to design symmetry and similar structures.

After that, the radiation pattern of the proposed antenna is measured using an anechoic chamber to validate the simulated results. Figure 7(a) shows the 3D radiation patterns of the proposed antenna. Figure 7(b) compares both simulated and measured 2D radiation patterns at frequencies 4.2 GHz, 6.85 GHz, and 10.2 GHz, respectively. The radiation patterns are measured in two planes, i.e. *E* and *H*. While measuring the pattern, only a single-port is excited at a time, and all other radiators are matched terminated with a load (50 Ω). The measured patterns are strongly mapped to the simulated; however, little tolerances might occur due to measurement imprecision. The plot reveals that the proposed antenna's radiation patterns exhibit orthogonal and mirror transformations. These results confirm that the designed radiator can offer good pattern diversity characteristics. Further, Fig. 7(c) illustrates the proposed antenna's realized gain and total efficiency for all ports. It is observed from the plots that peak gain and total efficiency of the proposed MIMO antenna for all elements are around 3 dBi and 80% over the operating band of frequencies except at the notched-band region, respectively.

Diversity characteristics

In this section, some crucial parameters like ECC, DG, and mean effective gain (MEG) have been observed to evaluate the diversity performance of the proposed MIMO antenna system. Figure 8(a) illustrates the simulated ECC between diagonal and

adjacent elements of the proposed antenna. ECC is calculated using both *S*-parameters and far-field methods. The following equation represents the ECC computation using a far-field approach [23]:

$$\rho_e(i, j) = \frac{\int_0^{2\pi} \int_0^\pi A_{i,j}(\theta, \phi) \sin\theta \, d\theta d\phi}{\sqrt{\int_0^{2\pi} \int_0^\pi A_{i,i}(\theta, \phi) \sin\theta \, d\theta d\phi + \int_0^{2\pi} \int_0^\pi A_{j,j}(\theta, \phi) \sin\theta \, d\theta d\phi}} \quad (4)$$

$$A_{i,j}(\theta, \phi) = XPR \cdot E_{\theta i}(\theta, \phi) E_{\theta j}^*(\theta, \phi) P_\theta(\theta, \phi) + E_{\phi i}(\theta, \phi) E_{\phi j}^*(\theta, \phi) P_\phi(\theta, \phi), \quad (5)$$

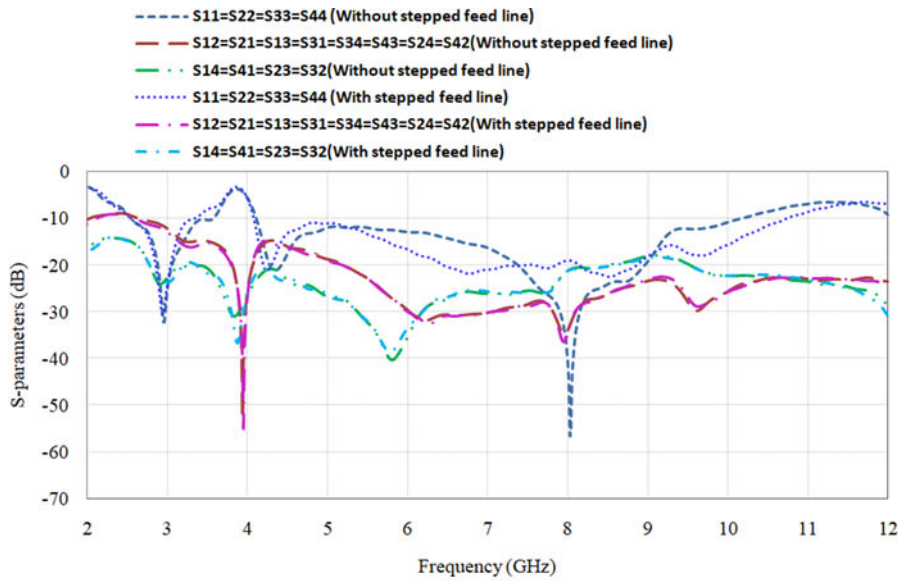
where XPR denotes the power ratio across elevation and azimuthal angle, also known as the cross-polarization ratio (P_V/P_H). The approach mentioned above is quite accurate but time-consuming. Another process that can be used for calculating ECC is with the *S*-parameters. This method is highly effective only in the case of certain assumptions and can be expressed as follows:

$$ECC_{ij} = \frac{|S_{ii}^* S_{ij} + S_{ji}^* S_{jj}|^2}{(1 - |S_{ii}|^2 - |S_{jj}|^2)(1 - |S_{jj}|^2 - |S_{ii}|^2)}. \quad (6)$$

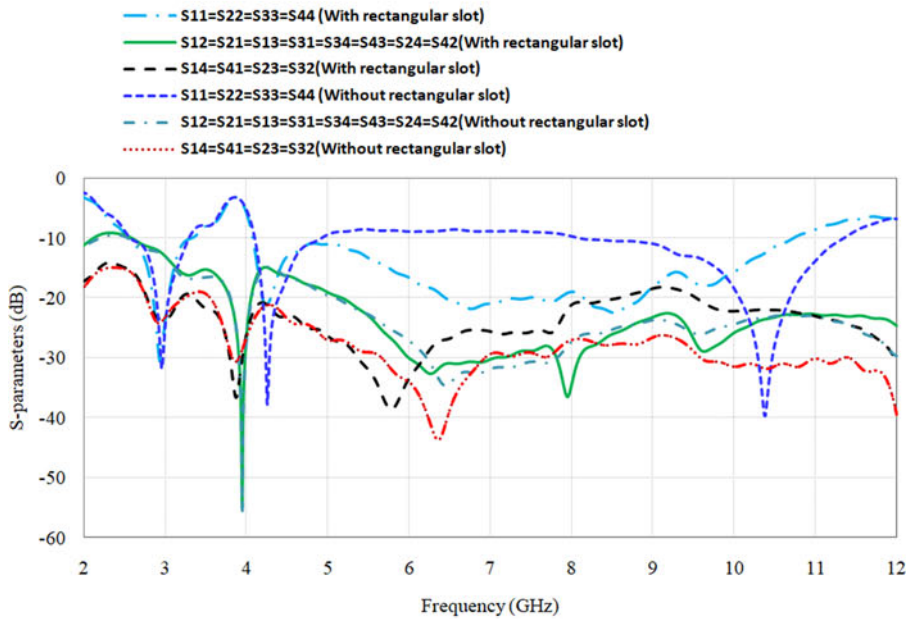
The plot reveals that ECC in the case of both adjacent and diagonal elements (far-field and *S*-parameters approach) is not more than 0.3 over the operating band. Its value should be real and varies from 0 to 1. In an ideal scenario, it should be equal to 0 but practically not more than 0.5. Further, to assess the enactment of the proposed diversity system, DG is observed. Figure 8(b) shows the DG for both adjacent and diagonal elements of the proposed antenna (using the far-field and *S*-parameters approach). The mathematical representation of DG in terms of ECC is described in the following equation [24]:

$$DG = 10\sqrt{1 - ECC}. \quad (7)$$

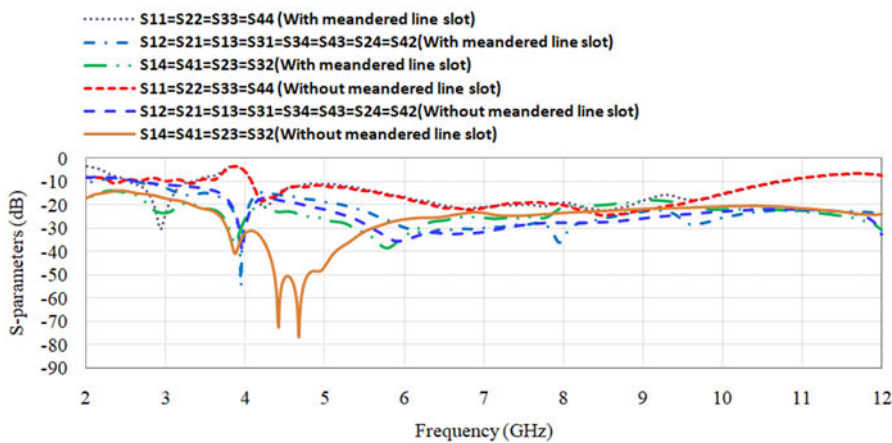
It is noticed from the above formula that both these parameters are directly linked, i.e. the higher the ECC, the lesser would



(a)



(b)



(c)

Figure 5. (a) S-parameters of the proposed antenna with and without stepped feed line. (b) S-parameters of the proposed antenna with and without rectangular slot. (c) S-parameters of the proposed antenna with and without meandered line slot.

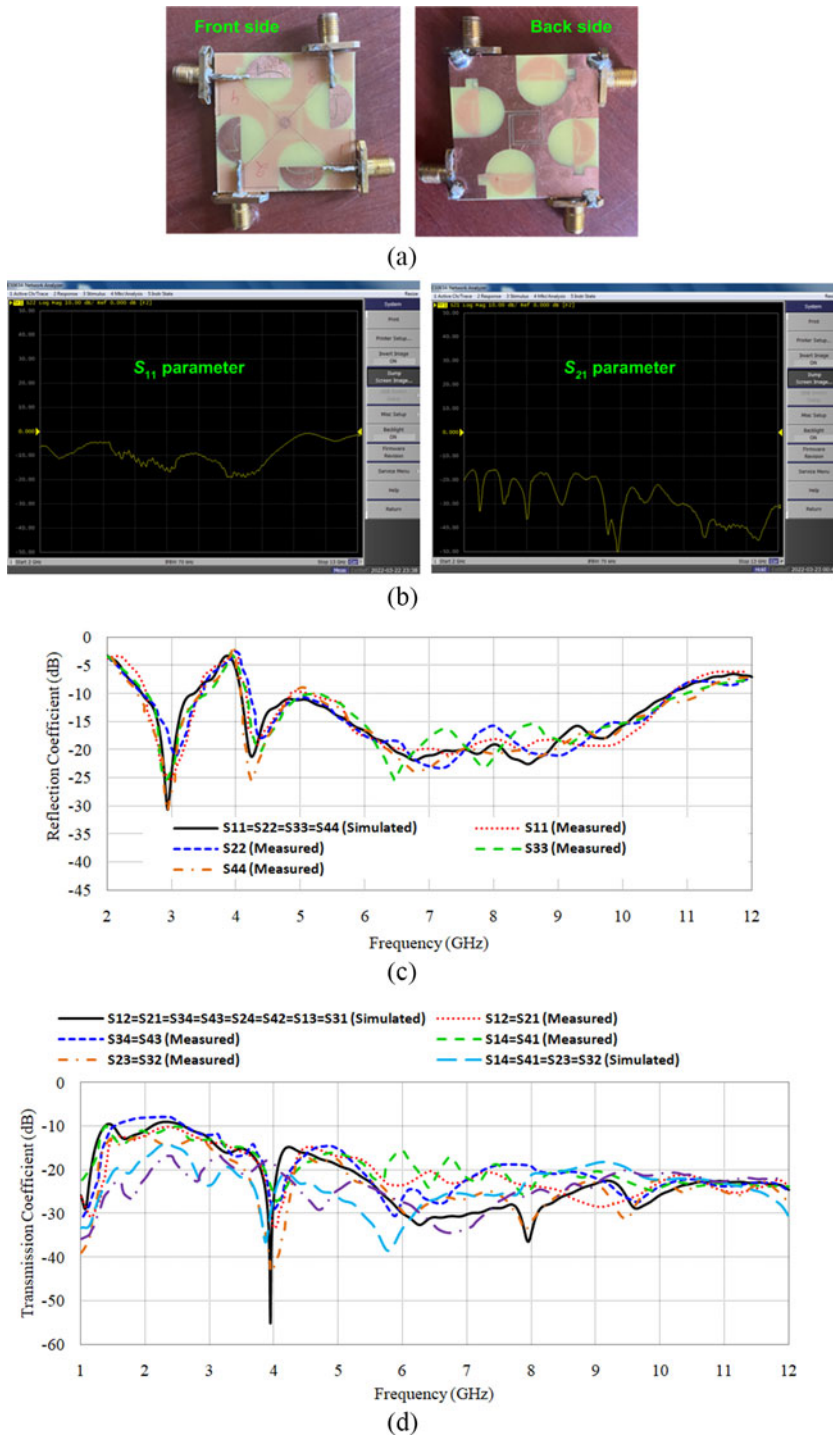


Figure 6. (a) Top and bottom layout of the proposed antenna. (b) Measured snapshot of S₁₁ and S₂₁. (c) Simulated and measured reflection coefficients of the proposed antenna. (d) Simulated and measured transmission coefficients of the proposed antenna.

be the DG or vice versa. Another important metric often utilized to review the diversity performance of the MIMO system is MEG. Figure 8(c) depicts the MEG of the proposed MIMO antenna with varying environmental conditions. MEG is the ratio of the received power to the impinging power of the antenna. Mathematically, it is described as [24]:

$$MEG = \int_0^{2\pi} \int_0^\pi \left(\frac{XPR}{1 + XPR} G_\theta(\theta, \phi) P_\theta(\theta, \phi) + \frac{1}{1 + XPR} G_\phi(\theta, \phi) P_\phi(\theta, \phi) \right) \sin\theta \, d\theta d\phi \quad (8)$$

Ideally, the ratio of MEG among the antenna elements should be close to unity. It is evident from the plot that MEG with different XPR values, i.e. 0 dB, 1 dB, and 5 dB for isotropic, indoor, and outdoor environmental conditions, respectively, satisfies the equality criterion of the diversity system.

Twenty-elements UWB-MIMO antenna configuration

This section illustrates the design and analysis of the 20-element UWB-MIMO antenna with band-notched characteristics from

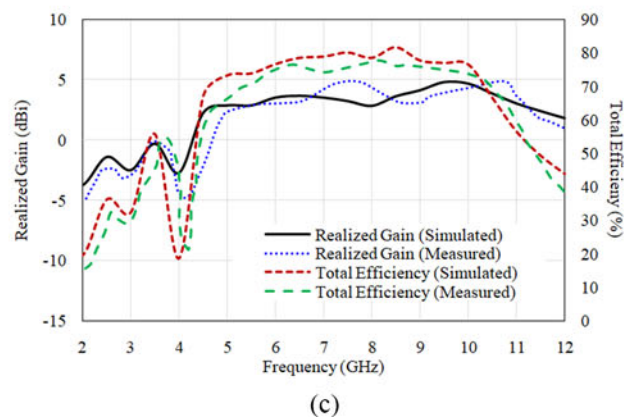
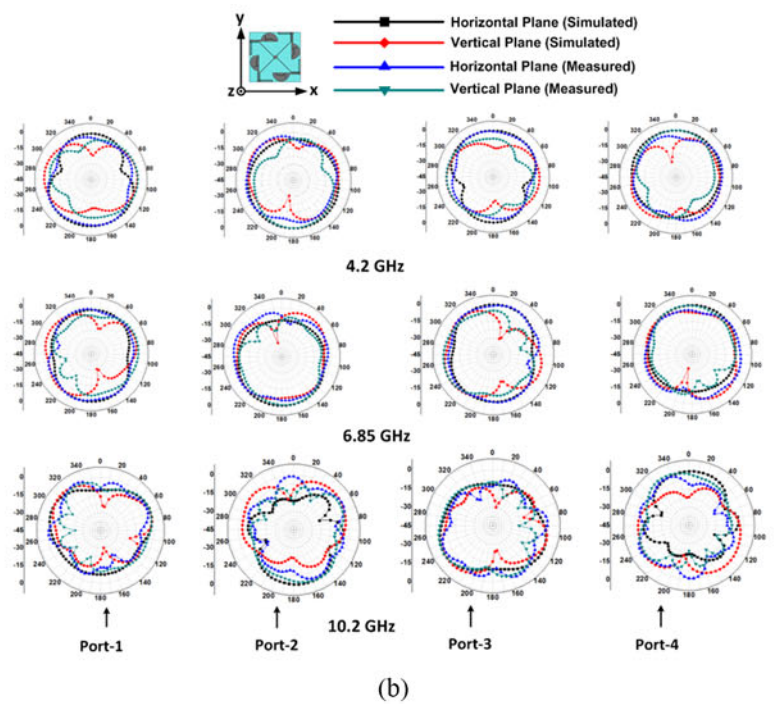
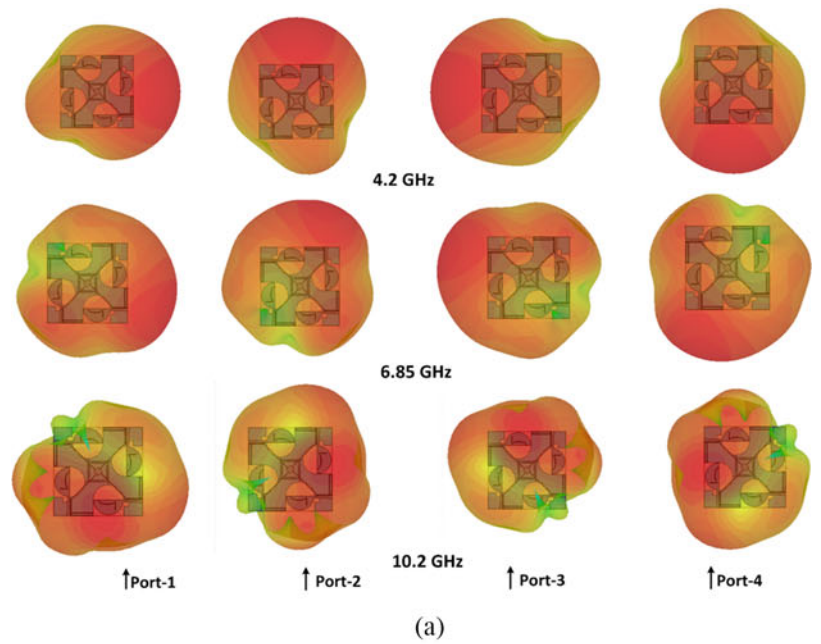


Figure 7. (a) 3D radiation pattern of the proposed antenna. (b) 2D radiation pattern (both simulated and measured) of the proposed antenna with band-notched characteristics at three frequencies. (c) Simulated realized gain and efficiency of the proposed antenna with band-notched characteristics.

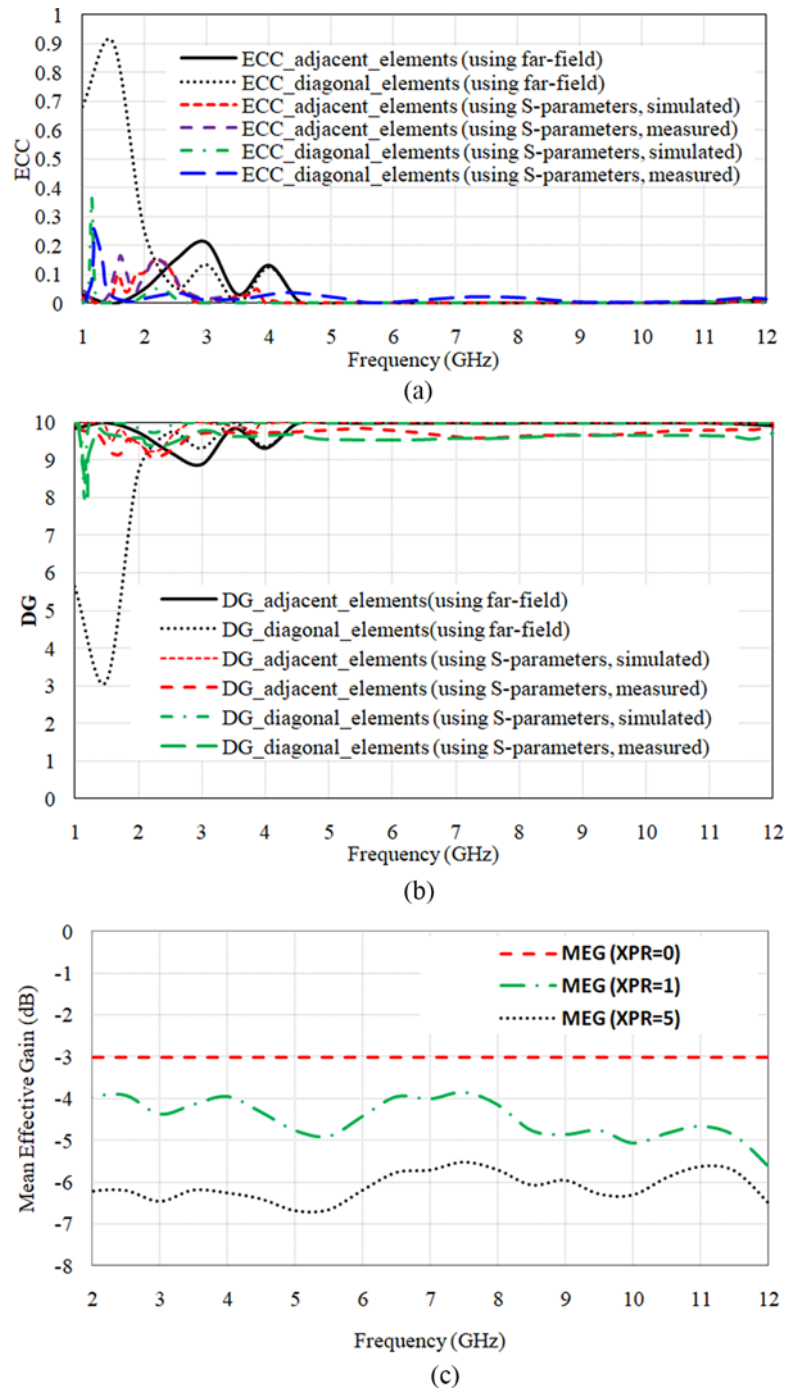


Figure 8. (a) Simulated ECC (using both far-field and S-parameter method) between diagonal and adjacent elements of the proposed antenna. (b) Simulated diversity gain (DG) (using both far-field and S-parameter method) of the proposed antenna. (c) Simulated MEG of the proposed antenna with different XPR values.

the proposed four-port as a unit cell. Its overall volume is $135 \times 135 \times 35 \text{ mm}^3$. The design consists of four unit cells (denoted as U1, U2, U3, and U4) that are orthogonally positioned at the top around the corners of a different unit cell (indicated as U5), as shown in Fig. 9(a). The center unit cell can act as a primary host in a localization system for connecting different devices. Figure 9(b) depicts the ground plane of the proposed 20-element antenna. A very thin metallic strip of 2 mm is used to attach the ground plane of all unit cells. As for real-time wireless applications, one must consider the shared ground plane effects. Further, Fig. 9(c) illustrates the 3D view of the proposed 20-port UWB-MIMO antenna structure in which five unit cells are integrated onto a polystyrene

material, which has an ϵ_r value equal to 2.6. Furthermore, a bonding material (also called glue) with a thickness of 0.8 mm has also been used to stick the unit cells onto a polystyrene block. All the dimensions and separation between unit cells have been optimized to attain the desired results. The simulated reflection and transmission coefficient curves for port-1 are depicted in Fig. 9(d). The simulated reflection coefficients S_{11} (to simplify the plot, $S_{1,1}$ notation is used) for port-1 are less than -10 dB over frequencies 2.35 to 10.67 GHz except at 3.22 to 4.03 GHz. The simulated transmission coefficients ($S_{1,2}$, $S_{1,3}$, $S_{1,4}$, $S_{1,5}$, $S_{1,6}$, $S_{1,7}$, $S_{1,8}$, $S_{1,9}$, $S_{1,10}$, $S_{1,11}$, $S_{1,12}$, $S_{1,13}$, $S_{1,14}$, $S_{1,15}$, $S_{1,16}$, $S_{1,17}$, $S_{1,18}$, $S_{1,19}$, and $S_{1,20}$) are more than -14 dB over the entire UWB spectrum. Due

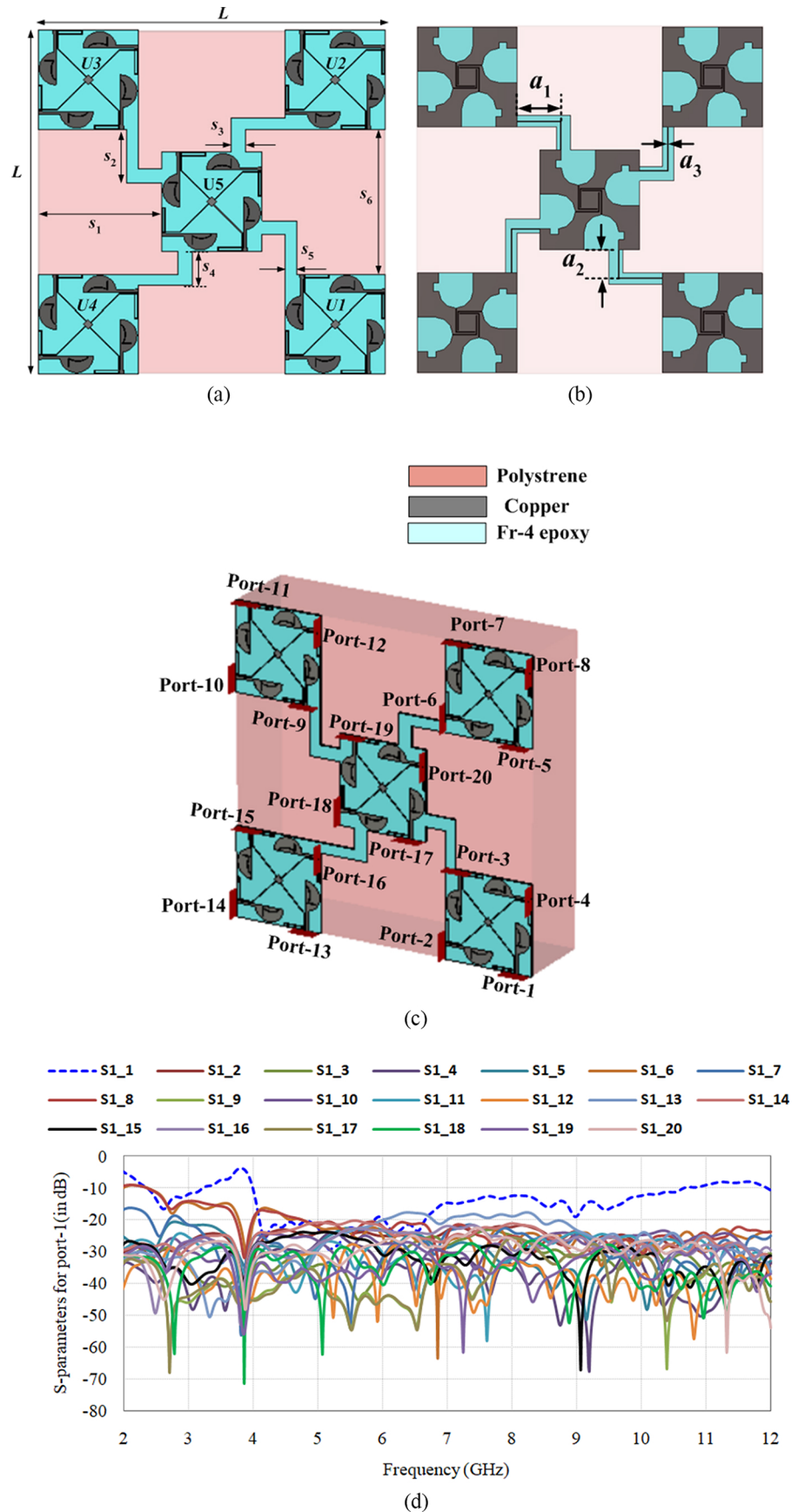


Figure 9. (a) Top layer of the proposed 20-element UWB-MIMO antenna with band-notched characteristics. (b) Bottom layout of the proposed 20-element UWB-MIMO antenna with band-notched characteristics. (c) 3D geometry of the proposed 20-element UWB-MIMO antenna with band-notched characteristics. (d) S-parameters of only port-1 of the proposed 20-element UWB-MIMO antenna with band-notched characteristics.

to the symmetricity of the antenna elements, S -parameters for all the antenna elements would nearly be the same. Moreover, the S -parameters plot curves of the 20-element UWB-MIMO antenna are nearly the same as that of the proposed quad-element UWB-MIMO antenna with band-notched characteristics. Hence, the utilization of the proposed 20-element UWB-MIMO antenna with band-notched characteristics can be considered a good candidate for wireless access point applications.

Conclusion

In this manuscript, a microstrip-fed compact quad-element UWB-MIMO antenna with WiMAX/C band-notched characteristics is presented. All four semicircular disc-shaped antenna elements are placed according to the orthogonal arrangement so that the incoming signals from both horizontal and vertical directions would enhance the system's link reliability as well as structure compactness. The radiators are etched with a reverse two-shaped slit to attain band-notched capability. The simulated reflection parameter results of the proposed antenna with band-notched characteristics are less than -10 dB over frequencies from 2.54 to 10.74 GHz with satisfactory isolation of more than -15 dB between diagonal and adjacent antenna elements. The proposed antenna's measured S -parameters and radiation patterns confirm good agreement with its simulated results. Also, the results reveal that ECC, MEG, EDG, and TARC values are acceptable. Then, a 20-element UWB-MIMO antenna is also studied for wireless access point applications. Satisfactory results were attained. Moreover, the proposed antenna is analyzed on the application platform (with the USB connector and large extended ground), ensuring its usefulness for wireless communication applications.

Acknowledgements. The authors would like to thank Antenna Research Laboratory, Department of Electronics and Communication Engineering, Thapar Institute of Engineering and Technology, Punjab, India, for providing the necessary instrument facility to carry out the measurement and seed money grant to carry out this work.

Competing interest. The authors declare that they have no known competing financial interests or personal relationships that could have appeared to influence the work reported in this paper.

References

1. Federal Communication Commission (FCC) (2002) First report and order on ultra-wideband technology. Washington, DC.
2. Li X, Bond EJ, Van Veen BD and Hagness SC (2005) An overview of ultra-wideband microwave imaging via space-time beamforming for early-stage breast-cancer detection. *IEEE Antennas and Propagation Magazine* **47**(1), 19–34.
3. Liu L, Cheung SW and Yuk TI (2013) Compact MIMO antenna for portable devices in UWB applications. *IEEE Transactions on Antennas and Propagation* **61**(8), 4257–4264.
4. Bekasiewicz A and Koziel S (2016) Compact UWB monopole antenna for internet of things applications. *Electronics Letters* **52**(7), 492–494.
5. Zhao H, Zhang F, Wang C and Zhang X (2014) A universal methodology for designing a UWB diversity antenna. *Journal of Electromagnetic Waves and Applications* **28**(10), 1221–1235.
6. Malviya L, Panigrahi RK and Kartikeyan MV (2017) MIMO antennas with diversity and mutual coupling reduction techniques: A review. *International Journal of Microwave and Wireless Technologies* **9**(8), 1763–1780.
7. Tang X and Chen ZN (2015) Simplification and implementation of decoupling and matching network with port pattern-shaping capability for two closely spaced antennas. *IEEE Transactions on Antennas and Propagation* **63**(8), 3695–3699.
8. Kayabasi A, Toktas A, Yigit E and Sabanci K (2018) Triangular quad-port multi-polarized UWB MIMO antenna with enhanced isolation using neutralization ring. *AEU - International Journal of Electronics and Communications* **85**, 47–53.
9. Khan A, Bashir S, Ghafoor S and Qureshi KK (2021) Mutual coupling reduction using ground stub and EBG in a compact wideband MIMO-Antenna. *IEEE Access* **9**, 40972–40979.
10. Hasan MN, Chu S and Bashir S (2019) A DGS monopole antenna loaded with U-shape stub for UWB MIMO applications. *Microwave and Optical Technology Letters* **61**(9), 2141–2149.
11. Amin F, Saleem R, Shabbir T, Rehman SU, Bilal M and Shafique MF (2019) A compact quad-element UWB-MIMO antenna system with parasitic decoupling mechanism. *Applied Sciences* **9**(11), 2371.
12. Singh HS, Kalraiya S, Meshram MK and Shubair RM (2019) Metamaterial inspired CPW-fed compact antenna for ultrawide band applications. *International Journal RF Microwave Computer-Aided Engineering* **29**(8), 1–9.
13. Sakli H, Abdelhamid C, Essid C and Sakli N (2021) Metamaterial-based antenna performance enhancement for MIMO system applications. *IEEE Access* **9**, 38546–38556.
14. Iqbal A, Saraereh OA, Ahmad AW and Bashir S (2017) Mutual coupling reduction using F-shaped stubs in UWB-MIMO antenna. *IEEE Access* **6**, 2755–2759.
15. Wang L, Du Z, Yang H, Ma R, Zhao Y, Cui X and Xi X (2019) Compact UWB MIMO antenna with high isolation using fence-type decoupling structure. *IEEE Antennas and Wireless Propagation Letters* **18**(8), 1641–1645.
16. Srivastava G and Mohan A (2016) Compact MIMO slot antenna for UWB applications. *IEEE Antennas and Wireless Propagation Letters* **15**, 1057–1060.
17. Yang B, Chen M and Li L (2018) Design of a four-element WLAN/LTE/UWB MIMO antenna using half-slot structure. *AEU—International Journal of Electronics and Communications* **93**(May), 354–359.
18. Modak S, Khan T and Antar YMM (2022) Miniaturized self-isolated UWB MIMO planar/cuboidal antenna with dual X-band interference rejection. *AEU—International Journal of Electronics and Communications* **143**, 154020.
19. Quddus A, Saleem R, and Bilal M (2016) Reconfigurable band-notched UWB-MIMO antenna, *2016 16th Mediterranean Microwave Symposium (MMS), Abu Dhabi, United Arab Emirates* **1**, 2–5.
20. Thakur E, Jaglan N, Gupta SD and Kanaujia BK (2019) A compact notched UWB MIMO antenna with enhanced performance. *Progress in Electromagnetics Research C* **91**(February), 39–53.
21. Gautam AK, Yadav S and Rambabu K (2018) Design of ultra-compact UWB antenna with band-notched characteristics for MIMO applications. *IET Microwaves, Antennas & Propagation* **12**(12), 1895–1900.
22. Yadav D, Abegaonkar MP, Koul SK, Tiwari V and Bhatnagar D (2018) A compact dual band-notched UWB circular monopole antenna with parasitic resonators. *AEU—International Journal of Electronics and Communications* **84**, 313–320.
23. Elshirkasi AM, Al-Hadi AA, Mansor ME, Khan R and Soh PJ (2019) Envelope correlation coefficient of a two-port MIMO terminal antenna under uniform and Gaussian angular power spectrum with user's hand effect. *Progress in Electromagnetics Research C* **92**(April), 123–136.
24. Singh HS, Agarwal M, Pandey GK and Meshram MK (2014) A quad-band compact diversity antenna for GPS L1/Wi-Fi/LTE2500/WiMAX/HIPERLAN1 applications. *IEEE Antennas and Wireless Propagation Letters* **13**, 249–252.



Harleen Kaur received her B.Tech. degree in electronics and communication engineering in 2014 from Lovely Professional University, Jalandhar, India, and M.E. in wireless communication engineering with specialization in speech signal processing in 2017 from Thapar University, Patiala, India. She is currently pursuing Ph.D. in ultra-wideband MIMO antennas for wireless applications at Thapar Institute of Engineering and Technology, Patiala, India. She has published eight

papers in reputed international conferences and journals. Her research interests include designing of compact ultra-wideband MIMO antennas for modern portable wireless communication devices, ultra-wideband MIMO antennas with band-notched characteristics, terahertz absorbers, and meta-material inspired antennas for multiband wireless applications.



Hari Shankar Singh was born in Sonbhadra (U.P.), India, in 1990. He received his B.Tech. degree from the IEC College of Engineering and Technology, Greater Noida (U.P.), India, in 2011 and Ph.D. degree from the Department of Electronics Engineering, Indian Institute of Technology (Banaras Hindu University), Varanasi, India, in 2015. Currently, he is working as assistant professor in the Department of Electronics and Communication Engineering, Thapar

Institute of Engineering and Technology, Patiala, Punjab, India. His Ph.D.

thesis has been awarded "Best Ph.D. Thesis" in the 3rd IEEE UPCON 2016 conference, held in IIT (BHU), Varanasi, from December 9 to 11, 2016. He has published 40 research papers in refereed International Journals and more than 50 research papers published/presented in national and international conferences/symposium/workshops. His research interests include microstrip antenna, MIMO antenna systems, ultra-wideband (UWB) antennas, electromagnetic bandgap (EBG) structure, RFID antennas, mobile antenna, and multiple antennas-user interactions. He has published more than 45 papers in various peer-reviewed international journals and conferences. He serves as a referee for various referred journals.



Rahul Upadhyay received his engineering degree in electronics and communication engineering from Rajiv Gandhi Technical University, Bhopal, India, and Ph.D. degree in signal processing from the Indian Institute of Information Technology, Jabalpur, India, in 2009 and 2016, respectively. Since late 2016, he has been working as assistant professor, Department of Electronics and Communication Engineering, Thapar Institute of Engineering and Technology, Patiala, India. Dr.

Upadhyay works in the area of Artificial Intelligence and Biomedical Image and Signal processing to develop assistive technological solutions. He completed his Postdoctoral Research with the Reilly Lab, Trinity College Institute of Neuroscience, Trinity College Dublin, Ireland. He has published many papers in journals and conferences of international repute. He has chaired and organized various international conferences and workshops and delivered keynote speeches.